3D Printed Parts of Polylactic Acid Reinforced with Carbon Black and Alumina Nanofillers for Tribological Applications

Article *in* Macromolecular Symposia · December 2020

DOI: 10.1002/masy.202000155

4 authors, including:

Paulo Henrique Machado Cardoso
Polimex Bioplásticos
8 PUBLICATIONS **98** CITATIONS

SEE PROFILE

Rossana M. S. M. Thiré
Federal University of Rio de Janeiro
104 PUBLICATIONS **2,378** CITATIONS

SEE PROFILE

Macromolecular Symposia
www.ms-journal.de

3D Printed Parts of Polylactic Acid Reinforced with Carbon Black and Alumina Nanofillers for Tribological Applications

*Paulo Henrique Machado Cardoso, Marcelo Ferreira Leão de Oliveira, Marcia Gomes de Oliveira, and Rossana Mara da Silva Moreira Thiré**

3D printing plays an important role in Industry 4.0 and has versatility to use different materials, including thermoplastic polymers. Polylactic acid (PLA), a bio-based biodegradable polymer, is used as a potential replacement for petroleum-based polymers in several applications, and is one of the most popular polymers used in 3D printing. Inorganic/organic nanoparticles can be incorporated in polymers to improve various properties such as thermal, mechanical, and tribological. This work investigates the effect of adding carbon black (CB) and alumina (ALM) nanofillers on the thermal, mechanical, and tribological properties of 3D printed PLA nanocomposites for tribological applications. Both nanofillers promoted progressive enhancement of thermal stability according to TGA. The improvement in the interaction between nanofillers and PLA matrix is revealed by an increase in viscosity of the nanocomposites. The nanocomposites containing 25%wt ALM and 75wt% CB presented better mechanical and wear properties, suggesting synergism between nanofillers and that CB may act as a compatibilizer between PLA and ALM. These results enable selecting the most suitable composition of nanofillers to be added to PLA to create filaments with better tribological properties.

1. Introduction

Additive manufacturing (AM), also known as 3D printing, is a revolutionary technology, mainly because it allows fabrication of virtually any complex shape by computer-aided design (CAD) of objects, which cannot be achieved through conventional methods.[1,2] 3D printing is based on layer-by-layer fabrication in which parts are constructed in a process of joining feedstock materials. AM plays an important role in Industry 4.0, saving time and costs, and is decisive for process efficiency by reducing complexity, allowing rapid prototyping and highly decentralized production processes, using a wide range of available nontoxic raw materials.[3–5]

P. H. M. Cardoso, R. M. da Silva Moreira Thiré
Program of Metallurgical and Materials Engineering, COPPE
Federal University of Rio de Janeiro – UFRJ
Caixa Postal 68505, Rio de Janeiro, RJ 21941-599, Brazil
E-mail: rossana@metalmat.ufrj.br
M. F. L. de Oliveira, M. G. de Oliveira
Materials Characterization and Processing Department
National Institute of Technology – INT
Rio de Janeiro RJ 20081–312, Brazil

DOI: 10.1002/masy.202000155

Among AM techniques, fused deposition modeling (FDM) is the most used technique. In this process, a filament is extruded at a temperature above its glass transition temperature and/or melting temperature through a moveable and heated nozzle head, and is deposited as a thread of molten material on a platform in three axis motion (x, y, z) according to the digital model. Then, the threads solidify to form a complete 3D part, in a layer by layer process. The movement of the extruder nozzle is guided by the tool path generated by the software.[5–7]

Polylactic acid (PLA) is one of the most popular polymers used in desktop 3D printers, since it has a relatively low melting temperature (150–160 °C), thus demanding less energy to print parts, besides having a low thermal expansion coefficient, which improves the printability by reducing the warp effect during the printing step.[8–10] PLA is a an aliphatic thermoplastic polyester that has several attractive properties, such as biodegradability, biocompatibility, excellent processability, and tensile and flexural strength and Young´s modulus comparable to conventional synthetic polymers, with relatively low cost. This polymer can be applied in surgical sutures, drug delivery systems, food packaging, textile fibers, films for agriculture, etc.[11–13]

The most critical disadvantage of parts fabricated via FDM is the reduction in mechanical properties relative to conventionally manufactured parts (e.g., injection-molded specimens) using the same materials.[14–16] To overcome the limited mechanical performance of 3D-printed pure polymer parts, new composite filaments are being studied and developed with enhanced properties. The evolution of nanocomposites has attracted strong interest among researchers since the addition of small amounts of nanofillers can improve several properties of the polymer matrix, such as mechanical and tribological properties and thermal stability.[17–21] Hence, polymeric nanocomposites in bulk form or as coatings are fast replacing metals and metallic/ceramic coatings in various demanding tribological applications (e.g., bearings) under dry sliding and lubricated conditions.[22] Inorganic nanofillers like alumina (Al_2O_3), silica, zinc oxide, titanium dioxide, nanoclays, carbon nanofibers, carbon nanotubes, graphite, and carbon black (CB) have been used in 3D printed materials.[20,21,23–25]

The use of metal oxide nanoparticles in the polymer matrix allows producing nanocomposites with improved thermal conductivity, high mechanical strength and stiffness, good thermal stability and wear resistance, among other features, in comparison with unfilled polymers. However, the presence of these hard metal oxide particles in micrometric size or in the form of agglomerates can increase the dry sliding friction coefficient of materials, leading to counterface abrasion, which is not desirable in solid lubricant bearing systems. Thus, it is important to understand the effects of filler dispersion and filler-matrix interfacial interactions in polymer nanocomposites for optimization of their tribological properties.[26,27]

Alumina (Al_2O_3) or aluminum oxide is an amphoteric oxide that exists in nature as the mineral corundum. It is frequently used as filler for polymer matrix nanocomposites.[23,26,28] An increase has been observed in wear resistance with rising alumina concentration in polytetrafluoroethylene (PTFE) composites.[28] Wetzel (2003)[29] showed that the addition of alumina nanoparticles in epoxy resin improves the wear resistance, stiffness, impact energy and failure strain at low filler contents (1–2 vol.%). Srinivasan[30] reported that the addition 3% alumina effectively reduced the frictional coefficient and consequently improved the wear resistance of epoxy/glass fiber nanocomposites. Bhimaraj[27] reported an increase in wear resistance in PET nanocomposites with 2% alumina addition. However, the main limitation of the use of alumina in engineering applications is its low fracture toughness.

Carbon nanostructures have been widely used as fillers to reinforce polymer matrices due to their mechanical strength, large surface area, and thermal stability, providing possible benefits in many potential technological and industrial applications, particularly those where tribological features are involved.[31–35] CB is the most common industrial carbon filler due to its relatively low cost, easy processing, and low specific weight in relation to the other types of fillers, such as carbon nanotubes. Moreover, it is frequently used as reinforcement for polymer matrices. CB consists of a fine black powder of nearly pure elemental amorphous carbon and has numerous applications in automotive products, inks, plastics and coatings. This nanofiller is produced by either partial combustion or thermal decomposition of gaseous or liquid hydrocarbons under controlled conditions, optimized to yield a variety of CB grades having specified ranges of properties (e.g., specific surface area, particle size and structure, conductivity, and color).[36–39]

CB has enhanced effects on the wear resistance of polymer-based nanocomposites. It stands out for its solid lubricating character when wear resistance is desired, since it reduces the coefficient of friction.[40–43] Khun et al.[43] observed that the addition of CB increased the friction coefficient in PA matrix nanocomposites and attributed this effect to the higher surface roughness. Dong et al.[41] reported that thermoplastic polyurethane/CB nanocomposites showed better wear resistance than pure thermoplastic polyurethane. Hassan[44] noted that CB resulted in an increase in the wear resistance of styrene-butadiene rubber (SBR) because of the improvement of mechanical properties.

From the tribological viewpoint, polymer nanocomposites have some advantages over micro-sized particle-reinforced composites. The material erosion is expected to be lower in nanocomposites since the nanofillers have similar size to the segments of the polymer chains. Besides this, the bonding between nanofiller and matrix is expected to be better than with microfiller due to its larger specific surface area.[45] Nanofillers can indirectly affect the tribology of polymer matrices by changing the crystallinity, microstructure, glass transition and degradation temperatures, and other physical/mechanical properties of the polymer.[27,45,46]

FDM 3D printed nanocomposites have not been fully studied. The objective of this work was to produce PLA nanocomposite filaments with improved mechanical and thermal properties and also improved wear resistance as a new feedstock for FDM, aiming at further application in tribology. PLA/alumina/CB filaments suitable for the FDM process were produced by an extrusion procedure. The new material was developed to combine the lubricity character of CB with load bearing capacity of alumina. The rheological, tribological, mechanical, and thermal properties of printed nanocomposite parts with different amounts of fillers were evaluated.

To the best of our knowledge, there are no papers recently published in the open scientific literature regarding the addition of alumina and CB as nanofillers in PLA for FDM applications.

2. Experimental Section

2.1. Materials

The commercial Ingeo Biopolymer 2003D PLA grade, produced by NatureWorks LLC and purchased from BASF, with a density of 1.24 g cm^{-3} was used as the matrix of the nanocomposites. SpectrAl 81 fumed alumina with high purity and an average diameter of 15–20 nm and Vulcan XC72R CB with an average diameter of 30–60 nm were supplied by Cabot, São Paulo, Brazil. All materials were used as received. PLA and nanofillers were dried at 80°C for 2 h before any melt processing.

2.2. Production of PLA/Carbon Black/Alumina Filaments

First, a twin-screw extrusion process was used to prepare the PLA/alumina (ALM)/CB nanocomposites with ALM/CB (%wt) proportions of 0/0, 100/0, 75/25, 50/50, 25/75, 0/100, with 3%wt of nanoparticles in relation to PLA. Samples were named PLAALMxCBy, where x and y are the amount of alumina and CB in nanocomposites, respectively. PLA/ALM/CB masterbatch extrusion was performed with a twin-screw extruder (model DRC 22, Extrusora Brasil), with a screw length-to-diameter (L/D) ratio of 36.4. FDM printing processes require highly consistent diameter of the filament. To assure the diameter accuracy, a further single screw extrusion process was conducted. Thus, the filaments were pelletized and re-extruded using a benchtop mini-extruder (model AX 16:26, AX Plásticos), with temperature zone settings of 140/180/190 °C and a nozzle diameter of 1.75 mm. The filament flow rate was set to 24.5 mm/s. The resulting filament diameter was 1.75 mm ± 0.10 mm. These filaments were used for FDM printing of the parts.

2.3. Fused Deposition Modeling of PLA/Carbon Black/Alumina Nanocomposites

PLA nanocomposite specimens were manufactured using a low-cost desktop 3D printer (model ST Cloner, Microbrás). CAD

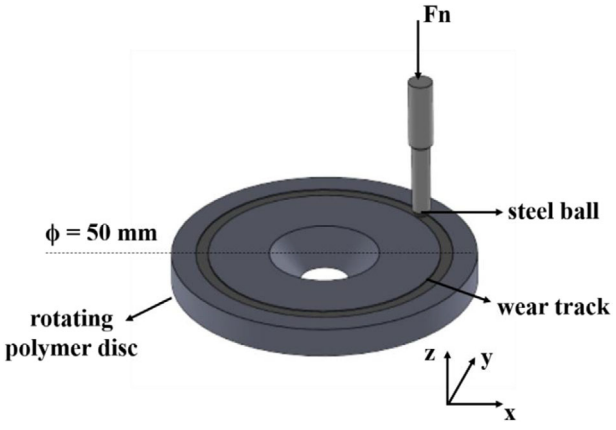

Figure 1. Ball-on-disc scheme.

models with dog-bone shape type V according to the ASTM D638-10 Standard[47] for tensile tests, and disc-shaped counter bodies (**Figure 1**) with 8 mm internal diameter, 50 mm external diameter, and 5 mm thickness for ball-on-disc tests were designed using SolidWorks software. All samples were printed with infill density of 100%, layer thickness of 0.1 mm, deposition speed of 40 mm s^{-1}, raster angles of ± 45°, and horizontal (xy plane) processing build direction. The same printing conditions were used for all the nanocomposites.

2.4. Characterization

2.4.1. X-ray Diffraction

X-ray diffraction analysis was performed with XRD diffractometer (model 6000, Shimadzu) operating with CuKα emission radiation (λ = 0.1542 nm) at 30 kV and 30 mA at room temperature. The diffraction patterns were collected in a 5°<2θ <40° scan range and at scan speed of 2°.min^{-1}.

2.4.2. Transmission Electron Microscopy (TEM)

The thin sections of samples were prepared using an RMC PowerTome XL Cryo-Ultramicrotome. Ultrathin sections (100 nm thickness) were cut from the central part of the 3D printed samples, in the plane parallel to the flow direction with a diamond knife at a temperature of 25°C and speed of 3 mm s^{-1}. These sections were collected on a 300 mesh copper grid for TEM analysis. The filler dispersion and morphology of ultrathin nanocomposite sections were evaluated by transmission electron microscopy (FEI Titan G2 80–200).

2.4.3. Rheometric Analysis

The rheological properties of pure PLA and nanocomposites were assessed with an AR-2000 rheometer (TA Instruments) using parallel-plate geometry with 20 mm diameter and a gap of 1.0 mm. Complex viscosity $\eta^*(\omega)$, storage modulus G'(ω), and loss modulus G''(ω) were determined using frequency sweep at 180 °C at frequencies varying from 0.01 to 100 rad.s^{-1} in nitrogen environment. A strain sweep of 0.1% to 700% (1 Hz) was also performed to determine the linear viscoelasticity range.

2.4.4. Thermogravimetric Analysis (TGA)

The 3D printed samples were analyzed with a Perkin-Elmer thermogravimetric analyzer, model STA 409C, using approximately 12 mg of sample weighed in an aluminum pan and heated between 30 and 700 °C at a rate of 10 °C.min^{-1} under nitrogen atmosphere with flow of 60 mL.min^{-1}.

2.4.5. Differential Scanning Calorimetry (DSC)

Thermal analyses were performed using a DSC Q100 calorimeter (TA Instruments). Nitrogen was used as purge gas at a flow rate of 20 mL.min^{-1}. Samples of about 5 mg were weighed and used in the analysis. They were first heated from 20 °C to 200 °C at a rate of 10 °C.min^{-1} to eliminate the thermal history and subsequently cooled to 20 °C at a rate of 10 °C.min^{-1}. The second heating cycle was conducted using the same conditions as the first cycle. From the second heating cycle's curve it was possible to obtain the cold crystallization temperature (T_{cc}), the melting temperature (T_m), the melting enthalpy (ΔH_f), and the cold crystallization enthalpy (ΔH_{cc}).

2.4.6. Tensile Properties

Tests of the produced parts were carried out according to the ASTM D638-10 Standard[47] at ambient temperature (23 ± 2 °C) and relative humidity of 50 ± 5%. The procedures were executed in a universal testing machine (Instron model 5582), with a constant displacement rate of 1 mm.min^{-1} and using a 5 kN load cell. Five samples of each formulation of nanocomposites were submitted to tensile loads parallel to the x-axis. Elastic modulus was determined as the angular coefficient of the tangent to the initial linear region of the stress-strain curve by linear regression analysis. The correlation coefficient was higher than 0.99. Toughness (or tensile energy to break) was measured by integrating the area under the stress-strain curve of the samples. The linear regressions and the integration of stress-strain curves were carried out with Origin 8.5.

2.4.7. Tribological Analysis

The tribological properties of the PLA matrix nanocomposites filled with different CB and alumina nanofiller contents were investigated using the ball-on-disc test by sliding against an SAE 5210 steel ball with 10 mm diameter in a wear track (circular path) with 15 mm radius for an approximate sliding distance of 1600 m at sliding speed of 0.3 m s^{-1} under a normal load (F_n) of 10 N using a commercial tribometer (Bruker UMT). The tribological test was carried out at room temperature using dry conditions. Three samples of each nanocomposite formulation were tested. Pure PLA and nanocomposite discs presented surface roughness (Ra)

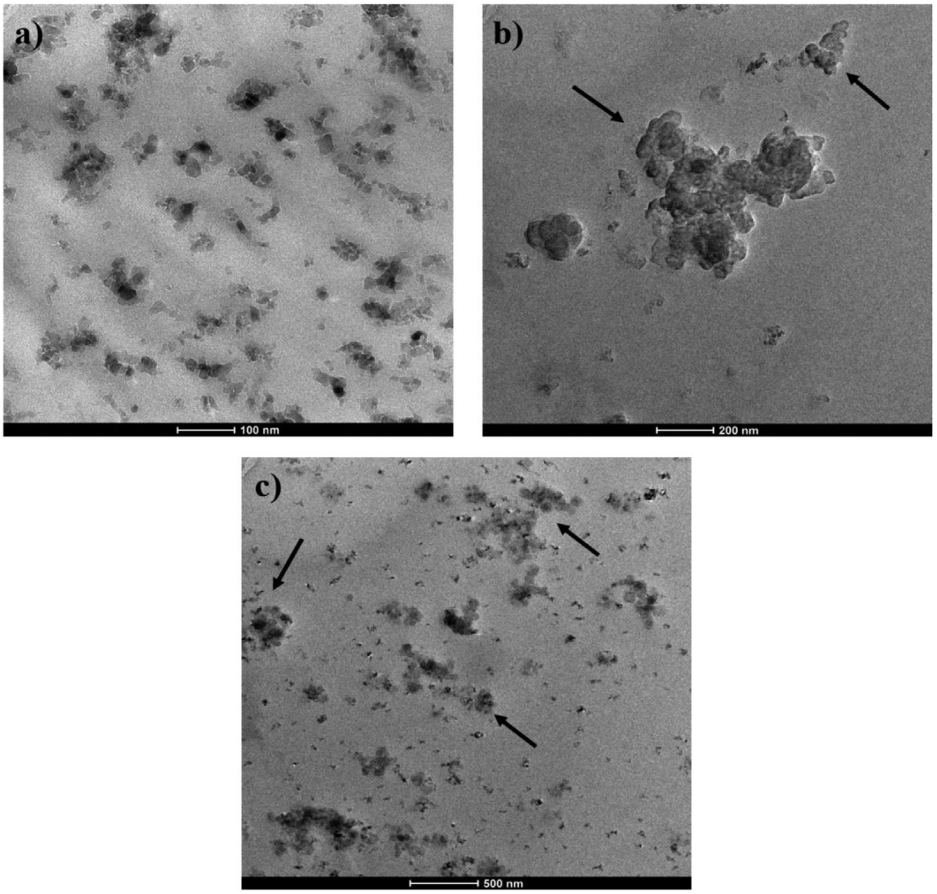

Figure 2. TEM images of the nanocomposites a) PLAALM100, b) PLACB100, and c) PLAALM25CB75.

of approximately 5 µm. The test method (Figure 1) was carried out according to ASTM G99-95.[48]

Prior to analysis, the initial mass of each nanocomposite test specimen was measured. After the test, the worn specimens were cleaned with tissue paper soaked with acetone and then air dried before measuring the final weight with an electronic analytic balance (Mettler Toledo, model AB 204). The difference in mass measured before and after the test gives the mass loss of the composite specimen during a particular sliding experiment. The specific wear rate of the specimens was calculated using Equation (1).[49]

$$\text{Specific wear rate}: Ks = \frac{\Delta m}{\rho L F n} \left(\text{mm}^3/\text{N-mm}\right) \quad (1)$$

where Δm is the mass loss during test duration (g), ρ is the density of the specimen (g/cm^3), L is the sliding distance (m), and Fn is the normal load (N).

2.4.8. Scanning Electron Microscopy (SEM)

The wear surfaces of specimens after the tribological tests were observed with a scanning electron microscope (model VEGA 3, Tescan) at an acceleration voltage of 20 kV. The cross-sections of tensile samples were also evaluated. All samples were gold coated prior to analysis.

3. Results and Discussion

3.1. X-Ray Diffraction

No changes in the diffraction pattern of the manufactured parts were observed despite addition of alumina and CB (data not shown). The diffractogram of all samples only showed an amorphous halo centered at around $2\theta = 16°$. In the FDM process, a fused thread is deposited onto the build platform to form the bottom layer. Since the build platform was maintained at room temperature, the deposited layer hardens quickly. Subsequent polymeric layers also cool fast. Due to low crystallization rate of PLA,[50] polymer molecules may not have enough time to properly organize themselves into crystallites, even in the presence of nanofillers.

3.2. Transmission Electron Microscopy (TEM)

Figure 2a–c present TEM images of ultrathin sections of 3D printed parts composed of PLAALM100, PLACB100 and PLAALM25CB75 nanocomposites, respectively.

The Al_2O_3 nanoparticles in PLAALM100 nanocomposite (Figure 2a) had nearly spherical morphology with flat faces, which is similar to that observed for metal oxides in the literature.[51] This image also shows that the alumina nanoparticles formed some nanometric agglomerates, homogenously distributed in the polymer matrix. This may indicate that fine alumina nanoparticles were dispersed in the PLA matrix.

Figure 2b shows that submicrometric agglomerates were formed by individual spherical nanoparticles, characteristic of CB. The typical bunch-like structure of round CB particles is evident (indicated by arrow).[52] Figure 2c reveals round and spherical particles of Al_2O_3 and CB in the PLA matrix (indicated by arrow). The alumina nanoparticles were adsorbed on the surface of CB agglomerates. This behavior has also been observed in other works.[53,54] In PLAALM25CB75 nanocomposite, alumina nanoparticles seem to be more dispersed than in PLAALM100 matrix. In spite of the formation of agglomerated structures in the samples, the particles' size (<200 nm) confirms the obtainment of nanostructured composites. In addition, good distribution of the nanoparticles in the PLA matrix was observed.

3.3. Rheometric Analysis

Understanding rheological properties is essential to determine the proper processing conditions for polymer extrusion and is of great relevance to determine the optimum balance between improvements in properties of extruded products and the processability of the materials. In this work, in order to mix hard particles with polymer, PLA nanocomposites were processed at high temperatures and high shear rates, mainly due to the considerable difference in densities. Determination of rheological properties of systems is important since adding solid particles in a molten polymer can modify the viscoelastic behavior, viscosity and elasticity of the system.

Figure 3a,b shows the curves (G' or G" versus angular frequency) obtained for the pure PLA and nanocomposite samples at 180 °C. The storage modulus (G′) is a sensitive rheological function related to the structural changes of nanocomposites.[55] Moreover, the storage modulus (G') at low frequency (ω) regime is strongly dependent on the addition of fillers, since the rheological properties at low ω regime reflect the relaxation and motion of the whole polymer chains.[56]

According to the rheological tests, for all samples both moduli increased with frequency, denoting typical viscoelastic behavior. The samples exhibited viscous effect predominant over elastic effect, since G" > G'. The addition of CB in the polymer matrix increased the viscosity of the system, probably due to disturbance of the flow lines and restriction of polymer chains mobility. This can be demonstrated by the change in dynamic melt rheological property of polymer nanocomposites with higher content of CB. The low-frequency G' increases by increasing CB loading, showing stronger adhesion with PLA matrix. This can be explained by the interaction between chemisorbed oxygen complexes (i.e., carboxylic acids, phenolic, quinonic, or lactonic groups) present in CB and the hydroxyl end groups of PLA during melt processing.[57,58]

In contrast, the addition of alumina nanoparticles (PLAALM100) decreased the G' value, indicating higher motion

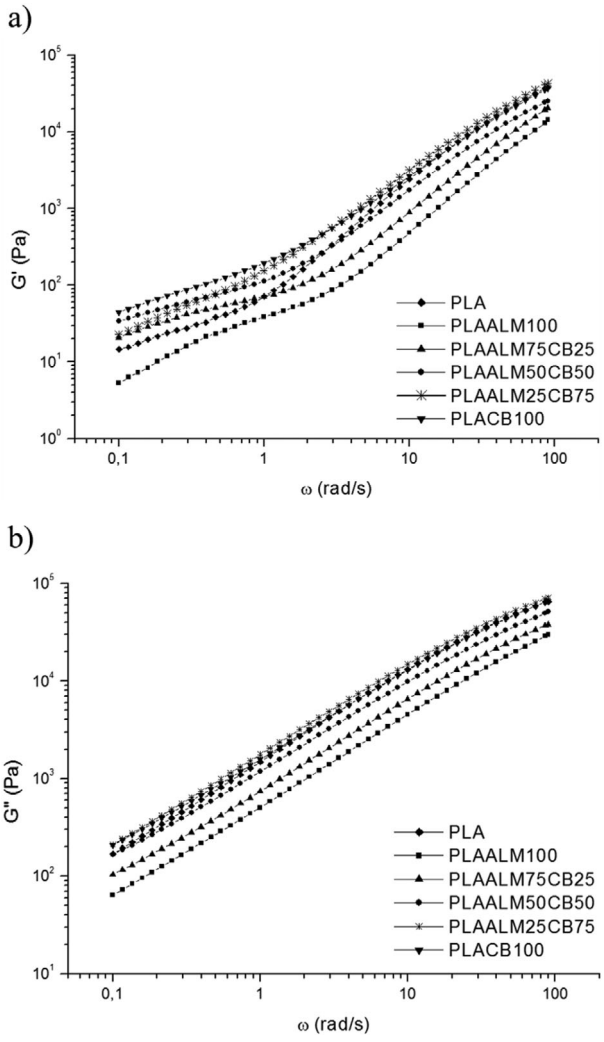

Figure 3. Curves from frequency sweep tests of pure PLA and nanocomposites: a) storage modulus; b) loss modulus.

of PLA chains. Since no surface treatment of alumina was carried out in this work, a weak interaction between matrix and nanofiller is likely. Furthermore, the terminal slope of G'-ω curve changed in the pure PLA at higher frequencies. Probably, the slippage movement among PLA molecules may have been impaired at short timescale.

The change of complex viscosity (η^*) as a function of deformation frequency for PLA and its nanocomposites is shown in **Figure 4**. Pure PLA presented non-Newtonian behavior at low frequency range and this behavior remained the same with addition of alumina and CB. All curves indicate a decrease in complex viscosity with increasing deformation frequency. The nanocomposites exhibited a slight shear thinning behavior at high angular frequencies due to the macromolecules' orientation and decrease of number of chain entanglements.[59]

In addition, higher complex viscosity was observed for nanocomposites with higher content of CB. The highest value was obtained by PLAALM25CB75, probably because of a synergistic effect between nanofillers, which can be explained by

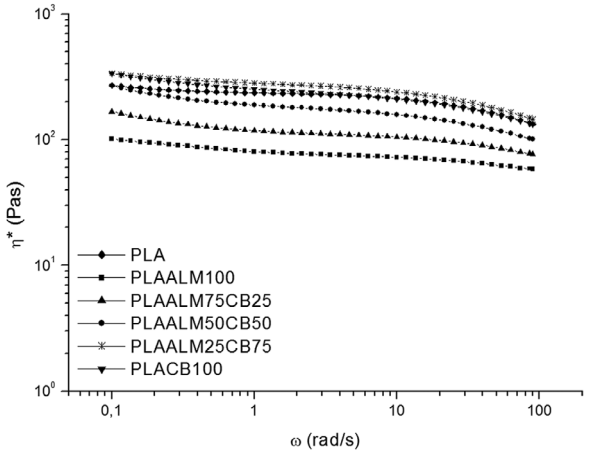

Figure 4. Complex viscosity of pure PLA and nanocomposites.

Table 1. Thermogravimetric analysis of PLA and its nanocomposites with alumina and carbon black.

Samples	Tonset [°C]	Tendset [°C]	Tmax [°C]	Residue [%]
Pure PLA	337.8	391.8	360.9	0.9
PLAALM100	347.6	390.7	374.8	2.7
PLAALM75CB25	348.2	393.5	376.7	3.4
PLAALM50CB50	355.7	395.4	381.9	3.6
PLAALM25CB75	363.1	397.2	386.6	3.5
PLACB100	364.4	404.6	385.9	4.2

the strong interaction between CB and PLA matrix and the adsorption of alumina nanoparticles on the CB surface, as already mentioned.

3.4. Thermogravimetric Analysis (TGA)

The degradation temperatures of pure PLA and its nanocomposites are shown in **Table 1**, which presents the values of initial degradation temperature (T_{onset}), temperature at maximum degradation rate ($_{Tmax}$) and final degradation temperature. All parameters were measured by TG and DTG curves (**Figures 5** and **6**).

In all curves, only one stage of thermal degradation was observed, ranging from 337 °C to around 404 °C. This behavior can be attributed to PLA mass loss as a result of hydrolytic cleavage of ester bonds.[60,61]

Table 1 shows that the addition of alumina and CB in the PLA matrix affected the thermal stability of the nanocomposites. Both nanofillers' addition increased the thermal degradation temperature, as already observed by other authors when alumina and CB were used separately.[43,62,63] Pure alumina addition increased the thermal degradation at around 14 °C, while the addition of pure CB resulted in an increase in thermal stability at around 25 °C. The increased thermal stability of nanocomposites can be related to the thermal insulation effect of alumina and CB and/or filler-matrix bonding, which may protect PLA molecules.

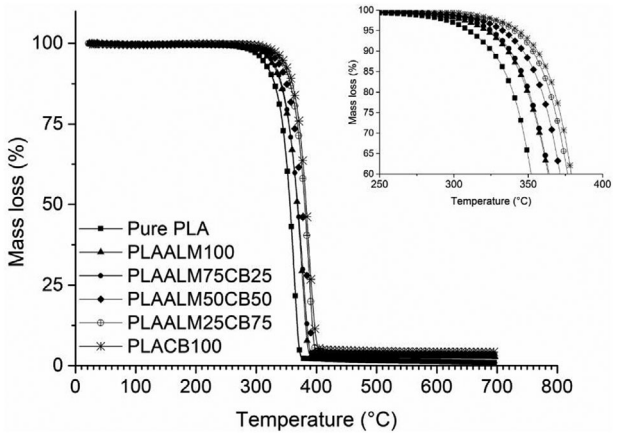

Figure 5. TG curves of PLA and its nanocomposites.

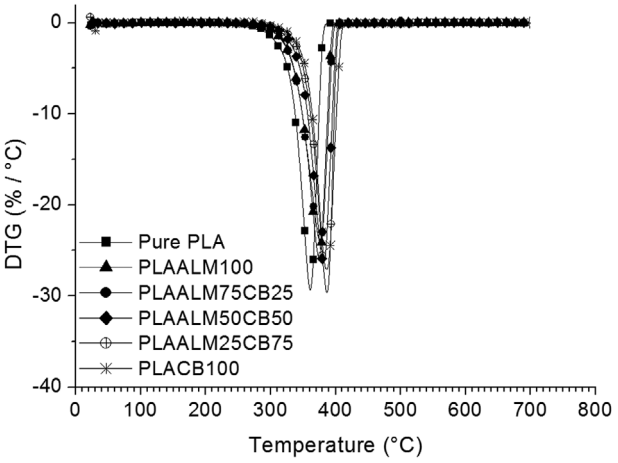

Figure 6. DTG curves of PLA and its nanocomposites.

Furthermore, as already shown by rheometric analysis, probably, there was a synergistic effect between alumina and CB nanofillers in the PLAALM25CB75 formulation, since it showed the highest thermal stability. The proper carbon filler content in the polymer matrix promoted higher thermal stability of the nanocomposites compared to pure matrix and other nanocomposites. It can be concluded that CB addition had a stronger effect on thermal stability than did the alumina nanofiller.

3.5. Differential Scanning Calorimetry

The melting and crystallization behavior of the pure PLA and its nanocomposites was monitored by DSC analysis during two heating cycles, where the samples' thermal history was erased in first heating cycle.

Figure 7 shows the DSC curves of pure PLA and PLA/alumina/CB nanocomposites with different contents obtained during the second heating cycle. The corresponding results for each analyzed sample are tabulated in **Table 2**. During the cooling cycle (not shown), no crystallization phenomena were observed for the pure PLA and its nanocomposites. There was only a change in baseline due to glass transition temperature.

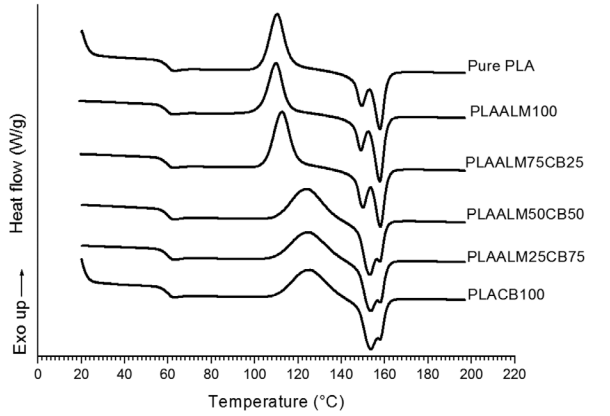

Figure 7. DSC curve obtained during the second heating cycle of pure PLA and its nanocomposites.

Table 2. DSC results from second heating cycle of pure PLA and its nanocomposites.

Samples	Tg [°C]	Tcc [°C]	ΔHcc [J/mol]	Tm1 [°C]	Tm2 [°C]	ΔHm [J mol^{-1}]
Pure PLA	60.6	110.4	29.9	149.1	152.6	30.9
PLAALM100	59.9	109.8	27.3	148.9	157.6	33.6
PLAALM75CB25	59.8	112.6	31.3	149.8	157.9	32.6
PLAALM50CB50	60.1	124.3	29.1	153.0	157.6	30.9
PLAALM25CB75	60.5	125.0	29.4	153.4	157.9	29.5
PLACB100	60.2	125.5	28.9	153.4	157.9	28.9

In the DSC curves of the second heating cycle (Figure 7), it was possible to observe three transitions for the pure PLA and all nanocomposites: glass transition temperature (Tg) at around 60 °C, an exothermic event corresponding to the cold crystallization temperature (Tcc), and finally an endothermic event related to the melting temperature (Tm). A fourth transition can be also observed, mainly in DSC curves of nanocomposites with higher content of CB (PLAALM50CB50, PLAALM25CB75 and PLACB100): a small exothermic peak, which appeared before double melting peaks.

Pure PLA showed a clear second-order transition (Tg) at 60 °C, after which it underwent one cold crystallization stage at Tcc1 = 110.4 °C and then two melting stages (Tm_1 and Tm_2) at 149.1 °C and 152.6 °C, respectively. This behavior was also observed by Kaygusuz and Özerinç (2019) and Abdulkhani et al. (2015).[64,65]

There was no significant difference in glass transition temperature (Tg) of pure PLA and its nanocomposites. This can indicate that incorporation of alumina and CB in PLA did not affect the start of coordinated movement of polymer molecules in the amorphous phase.

The cold crystallization temperatures (Tcc) observed for pure PLA and nanocomposites are related to the fact that PLA chains acquire reasonable mobility to disentangle from the amorphous phase and rearrange into ordered 3 D crystallites.[50] The exothermic peak observed in the vicinity of the melting transition is due to the melt-recrystallization mechanism of crystallites formed earlier. Pan (2009)[66] reported that the exothermic transition before the melting peak is due to transformation of the α' form crystal into α form upon heating, while other authors have reported that the recrystallization peak indicates that previously formed crystallites did not assume the stable orthorhombic α-crystal form in general.[50,64]

According to the literature, PLA can crystallize in two forms, the α and α' forms. A higher cold crystallization temperature (Tcc > 130 °C) induces the formation of the α form, whereas a low Tcc (80 °C < Tcc < 110 °C) leads to the formation of the α' form (disordered α form). In the range 110 °C < Tcc < 130 °C, the α and α' forms coexist. The measured values of cold crystallization temperature (Tcc) were in the range of 110.4–125.5 °C for pure PLA, in agreement with previous measurements by other researchers,[64,67] and its nanocomposites. This may indicate that α and α' forms coexisted in this study. The composite produced with 100% alumina (PLAALM100) and pure PLA presented similar Tcc. However, as the content of CB increased, the Tcc values also increased. This can be related to the impairment of PLA chain mobility caused by CB, as already discussed in the rheometric analysis. Thus, a higher temperature is necessary to provide enough energy for amorphous PLA chains to diffuse into an ordered crystal structure. Moreover, an increase in the area under the melt-recrystallization peak with higher content of CB can also be observed. This can be attributed to the hypothesis that CB promotes the growth of a higher quantity of crystals in stable α-form.

Pure PLA and PLA nanocomposites showed a distinct double endothermic peak (melting temperature), explained by the existence of two crystal forms (α and α'). This double endothermic peak is typical of polyesters[63] and is attributed to the formation of small and imperfect crystals that change into more stable crystals through melting and recrystallization (melt-recrystallization phenomenon) or to crystalline phases with two different crystallite populations.[67–69] Our results suggest that the first melting peak is due to the melting of crystals established during heating or during the recrystallization step at a temperature between 110°C and 130°C while the second peak corresponds to the melting of the more perfect crystals formed in the partially molten material.

For the PLAALM100 and PLAALM75CB25 nanocomposites, Tm1 (149 °C) was similar to that of pure PLA, probably due to the weak alumina-polymer interaction. The DSC results showed a slight increase in melting temperature (Tm1) for nanocomposites with higher content of CB (PLAALM50CB50, PLAALM25CB75, and PLACB100). The highest melting temperature in these three samples (Tm = 153 °C) may be related to the high crystallite quality (i.e., fewer defects, thicker lamellae, higher stability, etc.) due to the better interaction between CB and PLA.

3.6. Tensile Mechanical Properties

The Young's modulus (E), maximum tensile strength (σ_{TS}), and elongation at break (ϵ_b) of the pure PLA and nanocomposites are summarized in **Table 3**.

The material became more fragile and showed less tensile strength when the amount of alumina was maximum (PLAAM100). This can be explained by the low compatibility between the alumina nanofiller and PLA matrix. It has

Table 3. Tensile response values of pure PLA and all nanocomposites.

Samples	Young's Modulus [GPa]	Maximum Tensile Strength [MPa]	Elongation at Break [%]	Toughness [J m^{-1}]
Pure PLA	1.58 ± 0.00	39.01 ± 1.77	2.74 ± 0.11	0.58 ± 0.05
PLAALM100	1.50 ± 0.14	31.07 ± 3.95	2.19 ± 0.04	0.41 ± 0.00
PLAALM75CB25	1.61 ± 0.05	36.37 ± 5.84	2.53 ± 0.06	0.53 ± 0.01
PLAALM50CB50	1.61 ± 0.05	41.62 ± 1.46	2.74 ± 0.06	0.61 ± 0.01
PLAALM25CB75	1.67 ± 0.00	44.19 ± 1.82	2.83 ± 0.16	0.68 ± 0.08
PLACB100	1.60 ± 0.03	35.42 ± 3.13	2.26 ± 0.08	0.46 ± 0.04

been reported that alumina particles can only improve the tensile strength by having some prior surface treatments.[70] In contrast, an increase in tensile mechanical responses of PLAALMCB nanocomposites was observed as the CB content increased. With higher amount of CB, an increase in tensile strength and Young´s modulus was observed, particularly for PLAALM25CB75. These observations corroborate the hypothesis of synergism between the fillers, as proposed before.

Sanatgar (2017)[71] described strong adhesion between deposited PLA threads on the bottom PLA layer, explained by the highly effective diffusion of extruded PLA threads in the PLA part and the low interfacial tension due to the similar chemical nature of both and interpolymer polar interactions (Van der Waals dipole-dipole interactions) across phase boundaries. The synergism observed in PLAALM25CB75 probably promoted lower interfacial tension, contributing to the better adhesion of layers of this composite, and consequently higher tensile strength.

It can be suggested that toughness and strength properties derived from synergistic effect observed for PLAALM25CB75 overlapped the mechanical properties of PLACB100 due to the fact that alumina can facilitate the dispersion and distribution of CB nanoparticles in the PLA matrix, since the specific surface area (total surface area of a material per unit of mass) also increases. Since surface area increases, there is an increase in contact regions between CB and PLA, thus explaining the increased interfacial bonding. Despite the good adhesion shown by the rheological analysis of PLACB100, Figure 2b of the TEM analysis revealed the formation of typical bunch-like agglomerates of CB nanofillers, which diminish the specific surface area and thus decrease the CB attachment in the PLA matrix. Hence, for the

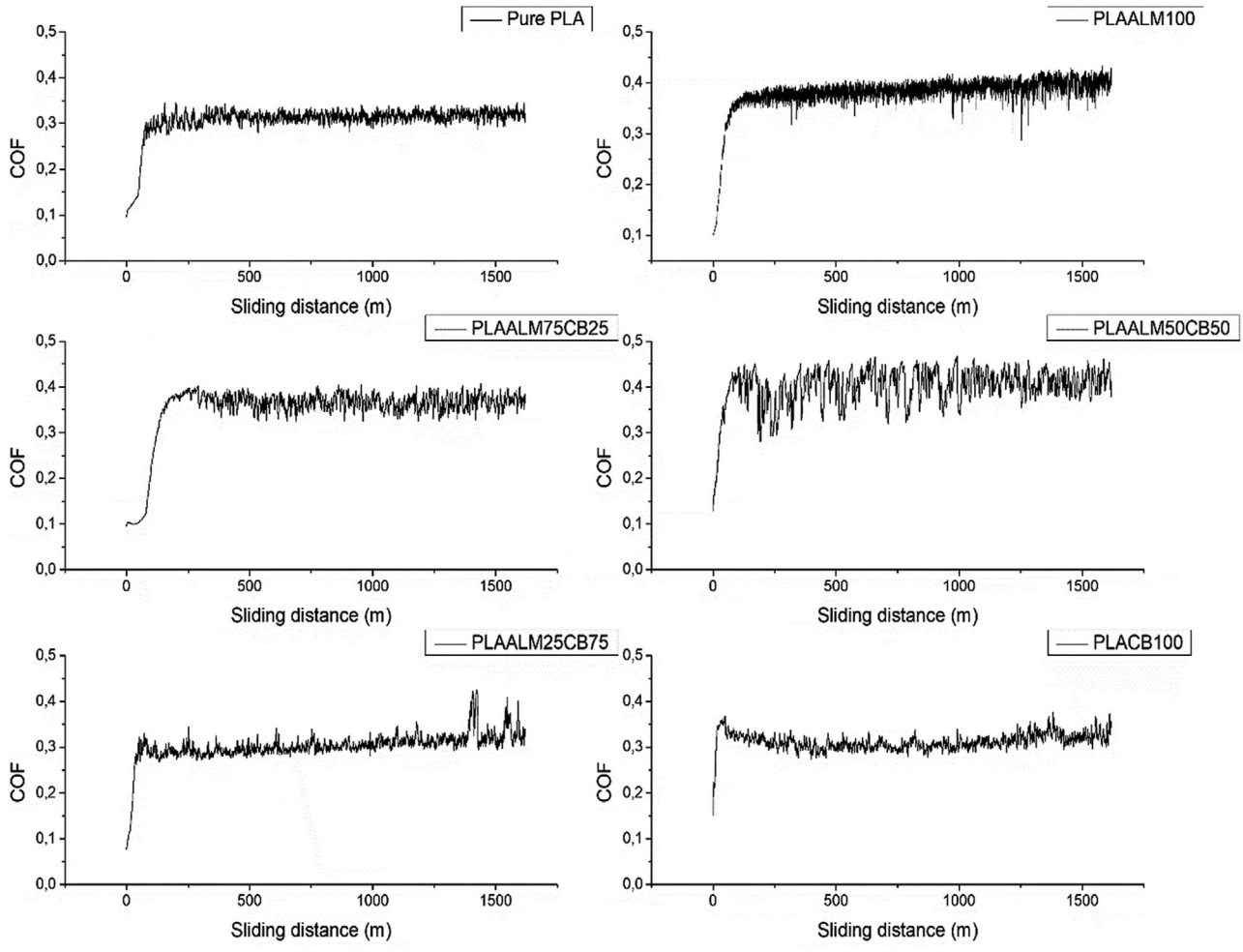

Figure 8. Coefficient of friction (COF) for pure PLA and nanocomposites.

Table 4. Wear properties of nanocomposites.

Samples	Average Friction Force (N)	Average Coefficient of Friction	Wear Rate [mm^3 $N.m^{-1}$]
Pure PLA	3.09 ± 0.43	0.30 ± 0.04	7.07×10^{-4}
PLAALM100	3.94 ± 0.60	0.39 ± 0.03	9.07×10^{-4}
PLAALM75CB25	3.75 ± 0.55	0.37 ± 0.03	7.88×10^{-4}
PLAALM50CB50	3.96 ± 0.47	0.39 ± 0.04	7.25×10^{-4}
PLAALM25CB75	3.11 ± 0.42	0.30 ± 0.03	6.90×10^{-4}
PLACB100	3.11 ± 0.41	0.31 ± 0.03	7.71×10^{-4}

nanocomposites fabricated just using CB as nanofiller, the increase in CB content contributes to the generation of large agglomerates, which can reduce the material's mechanical strength.

3.7. Tribological Properties

The tribological properties of the PLA matrix nanocomposites filled with different amounts of CB and alumina nanofillers were investigated using the ball-on-disc tribological test. **Figure 8** presents the wear profile by coefficient of friction graph as a function of sliding distance for pure PLA and the nanocomposites during the whole distance of the test.

Table 4 presents the average values of friction force (F_f) and coefficient of friction (COF), both measured in steady-state from friction graphs of the pure PLA and nanocomposites (Figure 8). The wear rate was calculated based on the method represented by Equation (1).

It is clear that at the beginning of the running-in stage, sliding performance was similar for pure PLA and all nanocomposites. The COF changed as a function of the sliding distance, as shown in Figure 8. The COF graphs show a transition from transient to steady-state wear behavior. A rapid rise of the COF at the initial stage was found for the pure PLA and all nanocomposites, which can be attributed to the increase of the contact area as the sliding continued, because of initial adhesion of pure PLA and nanocomposites to the steel surface. In this stage, the contact zone is being reformed and restructured (e.g., the topographic and surface layers).[72] After the transient state, the amount of transferred polymer debris tends to cover the metal surface more completely, and the COF tends to stabilize, since friction involves mainly polymer against polymer contact, called steady state.[73] A steady-state friction level was observed after the initial stage, indicating that the frictional force is characterized by the deformation of the surface under load and the consequent transfer of polymer debris to the metal contact surface. The deformation and fracture are caused by the stress state in the contact zone, which is damaged by normal load, contact geometry, and the coefficient of friction.[74]

Zhao (1999)[75] reported that some fillers improve the tribological behavior while others do not. In addition, Dasari (2009)[45] reported that tribological properties of polymers are generally improved with the addition of reinforcing and/or lubricating fillers. The latter author also explained that lubricating fillers lead to a weak bond in the material, and affect the strength of the materials, while reinforcing fillers increase the strength of polymeric materials but also increase the abrasiveness of the counterpart. Thus, increases of the coefficient of friction and counterface slider roughness can occur.

For the nanocomposites containing higher proportions of CB (PLAALM25CB75, PLACB100), the same values of F_f and COF were observed in relation to the pure PLA and lower values of F_f and COF in relation to the other nanocomposites. There may have been better dispersion of nanofillers in the PLA matrix for these nanocomposites explained by the interaction of the hydroxyls (-OH) present in the PLA with the CB carbon structure. During sliding, the CB nanofillers seen in a PLA matrix can be released and transferred to the interface between the composite and steel ball through the surface wear of the composite. The CB released served as a solid lubricant to reduce the friction of the composite, which dissipated frictional heat generated due to frictional sliding and promoted the formation of transfer debris on the metal counterface slider.[43,45,46] This result is in agreement with the increase of thermal stability in these nanocomposites. Increased thermal stability facilitated heat dissipation in the contact zone between the nanocomposites PLAALM25CB75 and PLACB100 and counterpart.

The wear graph results clearly indicated that the friction forces and friction coefficients of the nanocomposites with higher proportions of alumina (PLAALM100 and PLAALM75CB25) were higher than that of the pure PLA. Also, an increase in wear rate was observed. Dasari (2009)[45] reported that an uniform dispersion of nanoparticles is required to improve the friction and wear behavior of polymer nanocomposites under dry sliding. It appears that inhomogeneous distribution and dispersion of nanoparticles can result in extensive material loss due to disintegration of the particle agglomerates. However, homogenous dispersion of nanoparticles alone is not satisfactory to improve the wear resistance. It is also important to have good interfacial interactions of nano-alumina with the matrix in order to increase the wear resistance. In the present work, surface treatment of alumina was not applied, so good adhesion between alumina and PLA was not observed, as indicated by the rheological analysis. This led to interfacial debonding at weak interfaces and also interfacial debonding of the nano-alumina agglomerates, leading to higher wear loss volumes than for pure PLA and the other nanocomposites. This mechanism involves material detachment to form wear debris, caused by repeated sliding of the hard counterface asperities on the soft nanocomposite surface, thus resulting in abrasive damage in the form of intense plowing on the wear tracks.[26,45] This corroborates that higher proportions of alumina nanofiller are undesirable because they make the nanocomposites fragile, since this nanofiller is polar. Thus, high surface energy and high shear strength increase the friction coefficient and friction force.[45]

The calculated specific wear rate showed the same behavior seen for the friction force and friction coefficient of the nanocomposites. A higher content of CB nanofillers promoted a slight decrease in mass loss compared to the other nanocomposites, as shown by the decrease in specific wear rate.

These results were confirmed by the higher stiffness of the PLAALM25CB75 composite according to Young's modulus, corroborating the tribological analysis and the possible synergism between the fillers of this composite.

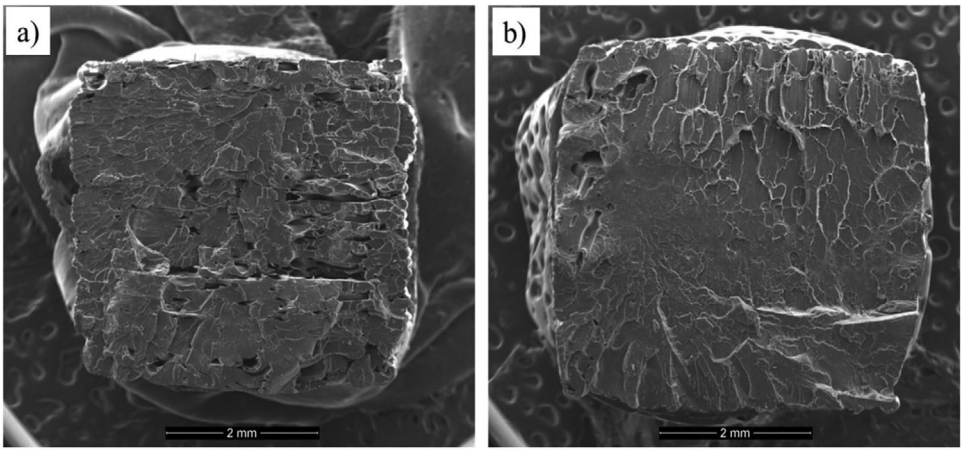

Figure 9. SEM images of tensile fracture surfaces of a) pure PLA and b) PLAALM25CB75 nanocomposite parts.

3.8. Scanning Electron Microscopy (SEM)

Figure 9a,b show the SEM images of the tensile fracture surface of pure PLA and PLAALM25CB75 nanocomposite parts.

Good interlayer adhesion was displayed by the bulk region generated by the FDM technique and revealed by SEM images. The fractured surface of bulk material exhibited a rough pattern, which may indicate that force per unit area reached a value at which plastic deformation of the materials occurred. Moreover, it can be inferred that the failure of those printed parts was mainly caused by rupture of deposited filaments instead of fracture of interlayer bonding. The interfacial bonding quality plays an important role in the microstructure and mechanical properties of the resulting parts. The addition of additives used in the PLA improved the printing performance of the nanocomposite PLAALM25CB75, as shown by the DSC results and the better adhesion on the nanocomposite specimen compared to the pure PLA. Also, voids can be observed in bulk PLA specimen in Figure 9a. These voids can act as stress concentration and consequently diminish the mechanical performance. Due to the better interfacial bonding between filaments in the PLAALM25CB75 (Figure 9b), this specimen presented improved mechanical performance in relation to pure PLA and nanocomposites with higher alumina content.

The worn surfaces were observed by SEM to identify some of the wear mechanisms in 3D printed parts with pure PLA and nanocomposites. **Figure 10**a–f show SEM images of the wear track of pure PLA and nanocomposites. The wear track of pure PLA and nanocomposites showed some delaminated regions, characteristic of adhesive wear, indicated by the presence of debris on the worn surfaces.[76] This is caused by the shearing due to the relative motion between the nanocomposites and counterface asperities. Frictional heat is generated by this process, inducing softening of the polymer, and then junctions are formed by the physical or chemical interactions of Van der Waals and hydrogen bonds of the polymer possibly due to heating at the interface, promoting detachment of particles. This mechanism may influence the friction and wear properties of the materials analyzed.[45,76]

The worn surfaces of pure PLA and PLAALM100 were rougher than the other nanocomposites, presenting larger debris particles and more total debris, respectively (Figure 10a,b), which corresponds to the relatively higher volume loss. These characteristics of the worn surface suggest that adhesive wear is the main reason for the wear loss of these nanocomposites.[77] The poor wear characteristic of the pure polymer is due to the softening process and subsequent debris generation and removal during sliding.[49,78] On the contrary, the SEM images showed a smoother surface and slightly enhanced wear resistance of the nanocomposites with higher content of CB, especially for PLAALM25CB75 (Figure 10e) in relation to the pure PLA and the other nanocomposites. The decreasing wear rates were accompanied by the small debris particle size and larger smooth area.[79] The wear rates of these nanocomposites found by tribology analysis may have decreased due to the lubricant effect of these particles with higher content of CB transferred to the counterface.[49,80] This result corroborated the lower friction coefficient, friction force and specific wear rate values measured in ball-on-disc test.

4. Conclusion

Good dispersion of the nanofillers in the PLA matrix was observed, although some agglomerates smaller than 200 nm were noted. The addition of alumina and CB nanofillers to PLA matrix increased the polymer's thermal stability. Furthermore, there was a synergistic effect between alumina and CB nanofillers in the PLAALM25CB75 formulation, resulting in an increase of around 25 °C in thermal stability.

The synergism observed in PLAALM25CB75 probably promoted the better adhesion of part layers, and consequently the higher tensile performance obtained. Tribological analysis revealed a lubricant character of CB, since nanocomposites with higher content of this nanofiller presented lower friction and force coefficients, as well as lower specific wear rate. However, the PLAALM25CB75 nanocomposite presented the best wear performance. An adhesive wear mechanism was detected by the SEM images of the nanocomposites' worn surfaces.

Thus, a novel 3D printed, bio-based filament for tribological applications was successfully obtained by incorporation of CB and alumina nanofillers in PLA. The results indicated that CB

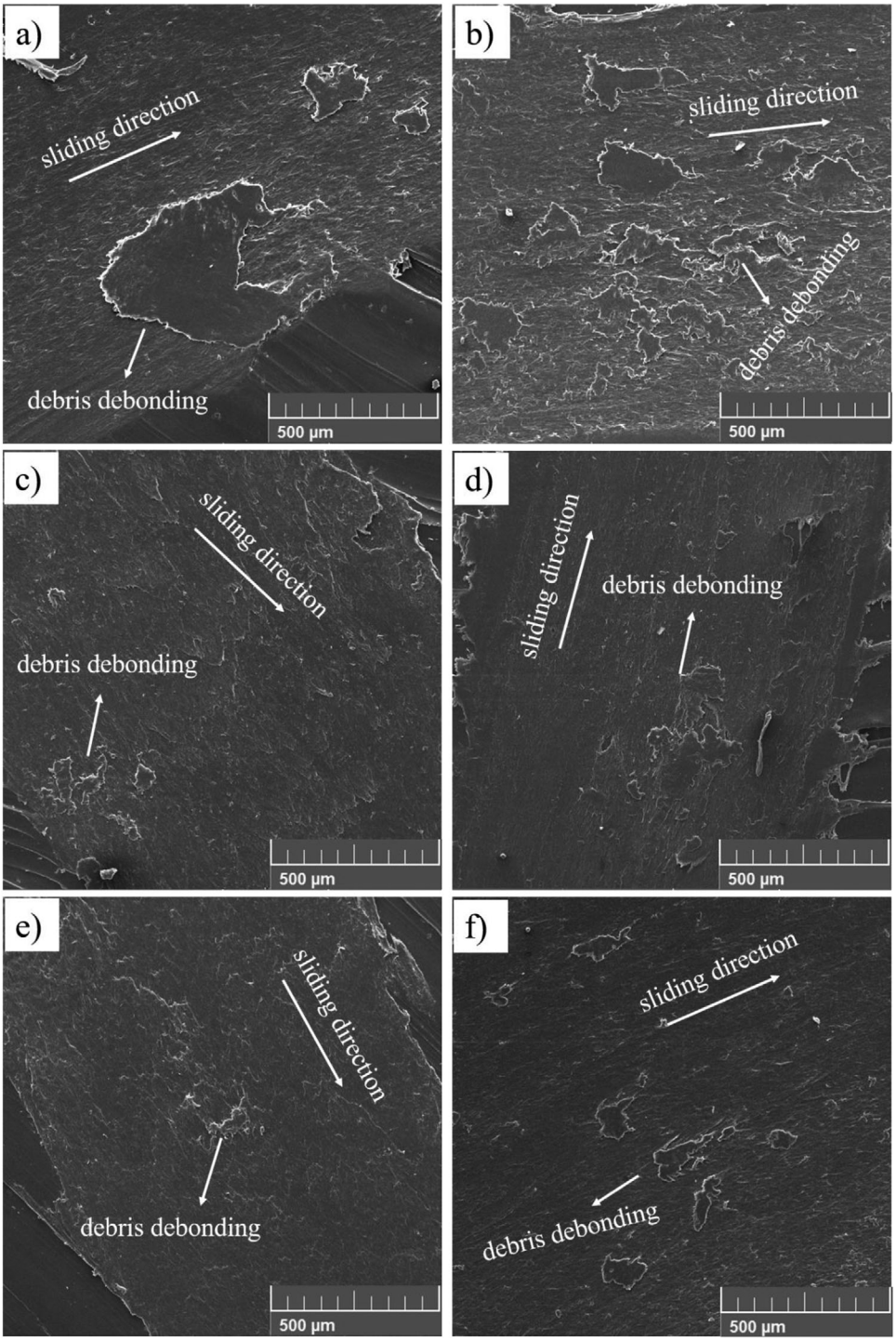

Figure 10. SEM wear track at 100x of a) pure PLA, b) PLAALM100, c) PLAALM75CB25, d) PLAALM50CB50, e) PLAALM25CB75, and f) PLACB100.

probably acted as a compatibilizer between the PLA matrix and alumina, especially when the 25:75 ALM:CB proportion was used.

Acknowledgements

P. H. M. Cardoso thanks Dr. Luiz Fernando Bastian (in memoriam) for his supervision and wise advice at the Nanocomposites Laboratory (PEMM/COPPE/UFRJ, Rio de Janeiro, Brazil). The authors thank the National Council for Scientific and Technological Development (CNPq) and the Carlos Chagas Filho Foundation for Supporting Research in the State of Rio de Janeiro (FAPERJ) for financial support, the Surface Phenomenon Laboratory (University of São Paulo, Brazil) for tribological analysis, and the Center for Characterization in Nanotechnology for Materials and Catalysis (CENANO) of the National Institute of Technology (INT) for TEM sample preparation.

Conflict of Interest

The authors declare no conflict of interest.

Keywords

carbon black, fused deposition modeling (FDM), nanocomposites, poly(lactic) acid, TEM

[1] K. Gnanasekaran, T. Heijmans, S. Bennekom, H. Woldhuis, S. Wijnia, G. With, H. Friedrich, *Appl. Mater. Today* **2017**, *9*, 21.
[2] P. Parandoush, D. Lin, *Compos.Struct.* **2017**, *182*, 36.
[3] D. Horst, C. Duvoisin, R. Vieira, *Inter. J. Eng. Technol. Res.* **2018**, *3*, 8.
[4] G. Liao, Z. Li, Y. Cheng, D. Xu, D. Zhu, S. Jiang, J. Guo, X. Chen, G. Xu, Y. Zhu, *Mater. Des.* **2018**, *139*, 283.
[5] O. A. Mohamed, S. H. Masood, J. L. Bhowmik, A. E. Somers, *J. Manuf. Process.* **2017**, *29*, 149.
[6] S. Berretta, R. Davies, Y. T. Shyng, Y. Wang, O. Ghita, *Polym. Test.* **2017**, *63*, 251.
[7] M. Dawoud, I. Taha, S. J. Ebeid, *J. Manuf. Process.* **2018**, *35*, 337.
[8] C. Casavola, A. Cazzato, V. Moramarco, G. Pappalettera, *Polym. Tes.* **2017**, *58*, 249.
[9] J. Torres, M. Cole, A. Owji, Z. DeMastry, A. P. Gordon, *Rapid Prototyping J.* **2016**, *22*, 387.
[10] B. Wittbrodt, J. M. Pearce, *Addit. Manuf.* **2015**, *8*, 110.
[11] M. A. Elsawy, K. Kim, J. Park, A. Deep, *Renewable Sust. Energ. Rev.* **2017**, *79*, 1346.
[12] E. Castro-Aguirre, F. Iñiguez-Franco, H. Samsudin, X. Fang, R. Auras, *Adv. Drug Delivery Rev.* **2016**, *107*, 333.
[13] k. Hamad, M. Kaseem, H. W. Yang, F. Deri, Y. G. Ko, *eXPRESS Polym. Lett.* **2015**, *9*, 435.
[14] G. Gomez-Gras, R. Jerez-Mesa, J. A. Travieso-Rodriguez, J. Lluma-Fuentes, *Mater. Des.* **2018**, *140*, 278.
[15] M. A. Ryder, D. A. Lados, G. S. Iannacchione, A. M. Peterson, *Compos. Sci. Technol.* **2018**, *158*, 43.
[16] J. M. Chacón, M. A. Caminero, E. García-Plazab, P. J. Núñez, *Mater. Des.* **2017**, *124*, 143.
[17] Y. Wang, Y. Mei, Q. Wang, W. Wei, F. Huang, Y. Li, J. Li, Z. Zhou, *Compos. Part B-Eng.* **2019**, *162*, 54.
[18] F. Daver, K. P. M. Lee, M. Brandt, R. Shanks, *Compos. Sci. Technol.* **2018**, *168*, 230.
[19] A. N. Dickson, K. A. Ross, D. P. Dowling, *Compos. Struct.* **2018**, *206*, 637.
[20] S. Dul, L. Fambri, A. Pegoretti, *Compos. Part A-Appl. S.* **2016**, *85*, 181.
[21] Z. Weng, J. Wang, T. Senthil, L. Wu, *Mater. Des.* **2016**, *102*, 276.
[22] M. U. Azam, M. A. Samad, *Tribol. Intern.* **2018**,*124*, 145.
[23] M. D. Kiran, H. K. Govindaraju, T. Jayaraju, *Mater. Today-Proc.* **2018**, *5*, 22355.
[24] R. T. L. Ferreira, I. C. Amatte, T. A. Dutra, D. Bürger, *Compos. Part B-Eng.* **2017**, *124*, 88.
[25] R. Singh, P. Bedi, F. Fraternali, I. P. S. Ahuja, *Compos. Part B-Eng.* **2016**, *106*, 20.
[26] S. Mallakpour, E. Khadem, *Prog. Polym. Sci.* **2015**, *51*, 74.
[27] P. Bhimaraj, D. L. Burris, J. Action, W. G. Sawyer, C. G. Toney, R. W. Siegel, L. S. Schadler, *Wear* **2005**, *258*, 1437.
[28] W. G. Sawyer, K. D. Freudenberg, P. Bhimaraj, L. S. Schadler, *Wear* **2003**, *254*, 573.
[29] B. Wetzel, F. Haupert, M. Q. Zhang, *Compos. Sci. Technol.* **2003**, *63*, 2055.
[30] V. Srinivasan, N. M. Raffi, R. Karthikeyan, V. Kalaichel, *J. Reinf. Plast. Compos.* **2010**, *29*, 3006.
[31] N. Jayanth, P. Senthil, *Compos. Part B-Eng.* **2019**, *159*, 224.
[32] Y. Quan, Q. Liu, S. Zhang, S. Zhang, *Appl. Surf. Sci.* **2018**, *445*, 335.
[33] W. Zhang, C. Cotton, J. Sun, D. Heider, B. Gu, B. Sun, T. W. Chou, *Compos. Part B-Eng.* **2018**, *137*, 51.
[34] H. Zhou, H. Wang, X. Du, Y. Zhang, H. Zhou, H. Yua, H. Y. Liu, Y. W. Mai, *Carbon* **2018**, *139*, 1168.
[35] F. Gutiérrez-Moraa, R. Cano-Crespoa, A. Rincónc, R. Morenod, A. Domínguez-Rodrígueza, *J. Eur. Ceram. Soc.* **2017**, *37*, 3805.
[36] I. Burmistrov, N. Gorshkov, I. Ilinykh, D. Muratov, E. Kolesnikov, S. A. Mazov, J. P. Issi, D. Kusnezov, *Compos. Sci. Technol.* **2016**, *129*, 79.
[37] E. Basavaraj, B. Ramaraj, J. H. Lee, Siddaramaiah, *Mater. Chem. Phys.* **2013**, *138*, 658.
[38] C. M. Long, M. A. Nascarella, P. A. Valberg, *Environ. Pollut.* **2013**, *181*, 271.
[39] N. Roy, R. Sengupta, A. K. Bhowmick, *Prog. Polym. Sci.* **2012**, *37*, 781.
[40] M. Ando, *Techl. Gaz.* **2018**, *25*, 1014.
[41] M. Dong, Q. Li, H.u Liu, C. Liu, E. K. Wujcik, Q. Shao, T. Ding, X. Mai, C. Shen, Z. Guo, *Polym* **2018**, *158*, 381.
[42] P. Junkong, P. Kueseng, S. Wirasate, C. Huynh, N. Rattanasom, *Polym. Test.* **2015**, *41*, 172.
[43] N. W. Khun, H. K. Feng, L. Li, E. Liu, *J. Polym. Eng.* **2018**, *35*, 367.
[44] H. H. Hassan, E. Ateia, N. A. Darwish, S. F. Halim, A. K. Abd El-Aziz, *Mater. Des.* **2012**, *34*, 533.
[45] A. Dasari, Z. Z. Yu, Y. W. Mai, *Mater. Sci. Eng.* **2009**, *63*, 31.
[46] K. Friedrich, *Adv. Ind. Eng. Polym. Res.* **2018**, *1*, 3.
[47] ASTM D638-14: Standard Test Method for Tensile Properties of Plastics **2014**.
[48] ASTM G99-17: Standard Test Method for Wear Testing with a Pin-on-Disk Apparatus **2017**.
[49] P. K. Bajpai, I. Singh, J. Madaan, *Wear* **2013**, *297*, 829.
[50] T. Farid, *IOP Conf. Ser.: Mater. Sci. Eng.* **2018**, *369*, 012031.
[51] S. Benykhlef, A. Bekhoukh, R. Berenguer, A. Benyoucef, E. Morallon, *Colloid Polym. Sci.* **2016**, *294*, 1877.
[52] S. Filizgok, M. Kodal, G. Ozkoc, *Polym. Compos.* **2018**, *39*, 2705.
[53] M. M. Rahmana, M. M. Alamc, A. M. Asiria, *J. Ind. Eng. Chem.* **2018**, *65*, 300.
[54] H. Yina, Q. Dai, X. Hao, W. Huanga, X. Wanga, *Surf. Coat. Technol.* **2018**, *352*, 411.
[55] C. Aumnate, S. Limpanart, N. Soatthiyanon, S. Khunton, *eXPRESS Polym. Lett.* **2019**, *13*, 898.
[56] J. Gong, N. Tian, X. Wen, X. Chen, J. Liu, Z. Jiang, E. Mijowska, T. Tang, *Polym. Degrad. Stab.* **2014**, *104*, 18.
[57] P. A. Delgado, J. P. Brutman, K. Masica, J. Molde, B. Wood, *J. Appl. Polym. Sci.* **2016**, *133*, 43926.
[58] D. Wu, Q. Lv, S. Feng, J. Chen, Y. Chen, Y. Qiu, *Carbon* **2015**, *95*, 380.
[59] M. C. Righetti, P. Cinelli, N. Mallegni, C. A. Massa, M. Irakli, A. Lazzeri, *Sustain* **2019**, *11*, 2783.
[60] G. Gorrasi, R. Pantani, *Adv. Polym. Sci.* **2018**, *279*, 119.
[61] J. M. Campos, A. M. Ferraria, A. M. B. Rego, M. R. Ribeiro, A. B. Timmons, *Mater. Chem. Phys.* **2015**, *166*, 122.
[62] Z. Lule, H. Ju, J. Kim, *Ceram. Int.* **2018**, *44*, 13530.
[63] T. F. Silva, F. Menezes, L. S. Montagna, A. P. Lemes, F. R. Passador, *J. Appl. Polym. Sci.* **2019**, *136*, 47273.
[64] B. Kaygusuz, S. Özerinç, *J. Appl. Polym. Sci.* **2019**, *136*, 48154.
[65] A. Abdulkhani, J. Hosseinzadeh, S. Dadashi, M. Mousavi, *Cell. Chem. Technol.* **2015**, *49*, 597.
[66] P. Pan, Y. Inoue, *Prog. Polym. Sci.* **2009**, *34*, 605.
[67] C. Courgneau, S. Domenek, R. Lebossé, A. Guinault, L. Avérous, V. Ducruet, *Polym. Int.* **2012**, *61*, 180.
[68] M. P. Arrieta, E. Fortunati, F. Dominici, E. Rayón, J. López, J. M. Kenny, *Carbohyd. Polym.* **2014**, *107*, 16.
[69] N. Bitinis, E. Fortunati, R. Verdejo, J. Bras, J. M. Kenny, L. Torre, M. A. L. Manchado, *Carbohyd. Polym.* **2013**, *96*, 621.
[70] K. Raza, M. Shamir, M. K. A. Qureshi, A. S. Shaikh, M. Z. Abdein, *J. Thermoplast. Compos. Mater.* **2018**, *31*, 291.

[71] R. H. Sanatgar, C. Campagne, V. Nierstrasz, *Appl. Surf. Sci.* **2017**, *403*, 551.
[72] G. Kalácska, *eXPRESS Polym. Lett.* **2013**, *7*, 199.
[73] L. Boissonnet, B. Duffau, P. Montmitonnet, *Wear* **2012**, *286-287*, 55.
[74] S. Bahadur, *Wear* **2000**, *245*, 92.
[75] Q. Zhao, S. Bahadur, *Wear* **1999**, *225-229*, 660.
[76] J. Bustillos, D. Montero, P. Nautiyal, A. Loganathan, B. Boesl, A. Agarwal, *Polym. Compos.* **2018**, *39*, 3877.
[77] H. Wang, L. Chang, X. Yang, L. Yuan, L. Yuan, Y. Zhu, A. T. Harris, A. I. Minett, P. Trimby, K. Friedrich, *Carbon* **2014**, *67*, 38.
[78] U. Nirmal, J. Hashim, M. M. H. M. Ahmad, *Tribol. Int.* **2015**, *83*, 77.
[79] D. R. Haidar, J. Ye, A. C. Moore, D. L. Burris, *Wear* **2017**, *380-381*, 78.
[80] N. Sharma, S. N. Alam, B. C. Ray, S. Yadav, K. Biswas, *Wear* **2020**, *418*, 290.